

Complexity=Anything in Gauss-Bonnet Gravity: Constraints and Phase Transitions

Xuanhua Wang,^{a,*} **Ran Li**,^{b,*} **Jin Wang** ^{c,d,*}

^a *Center for Theoretical Interdisciplinary Sciences, Wenzhou Institute, University of Chinese Academy of Sciences, Wenzhou, Zhejiang 325001, China*

^b *School of Physics, Henan Normal University, Xinxiang, Henan 453007, China*

^c *Department of Chemistry, Stony Brook University, Stony Brook, NY 11794, USA*

^d *Department of Physics and Astronomy, Stony Brook University, Stony Brook, NY 11794, USA*

E-mail: wangxh@ucas.ac.cn, liran@htu.edu.cn, jin.wang.1@stonybrook.edu

ABSTRACT: It has been proposed that quantum complexity is dual to the volume of the extremal surface, the action of the Wheeler-DeWitt patch, and the spacetime volume of the patch. Recently, a generalized volume-complexity observable was formulated as an equivalently good candidate for the dual holographic complexity. This proposal is abbreviated as “complexity=anything.” This proposal offers greater flexibility in selecting extremal surfaces and evaluating physical quantities, e.g., volume or action, on these surfaces. In this study, we explore the ‘complexity=anything’ proposal for Gauss-Bonnet black holes in asymptotic anti-de Sitter space in various dimensions. We demonstrate that this proposal guarantees the linear growth of the generalized volume at late times, regardless of the coupling parameters for four-dimensional Gauss-Bonnet gravity. However, this universality does not hold for higher dimensions. Moreover, discontinuous deformations of the extremal surfaces emerge when multiple peaks exist in the effective potential, which is reminiscent of a phase transition. Additionally, we present constraints on the coupling parameters of five-dimensional models in order for the generalized volume to be a viable candidate for holographic complexity.

*Corresponding authors

Contents

1	Introduction	1
2	Gauss-Bonnet-AdS black holes	3
3	CAny	4
4	Codimension-one extremal slices for Gauss-Bonnet in 4D	6
4.1	Existence of local maxima	6
4.2	Dipping and non-Dipping branches	8
4.3	Phase transition of the extremal slice	9
5	Codimension-one extremal slices for Gauss-Bonnet in 5D	11
5.1	Existence of local maxima	11
5.2	Couplings outside the allowed range	13
6	Discussion	15

1 Introduction

The holography of black holes has triggered much excitement and progress in our understanding of black holes over the last decade. The core of this treatment is validity of the central dogma, which states that black holes can be treated as standard quantum systems exhibiting unitary evolutions [1]. It is known that the entanglement entropy of a black hole is encoded in the area of its horizon after the Page time [2, 3]. While the entropy of a black hole increases only for a finite duration before reaching thermalization, the volume of its interior and the length of the wormhole for a two-sided AdS black hole continue to grow [4]. Consequently, it was suggested that a new quantum information measure is needed to capture the growth of the wormhole. Various concepts have emerged in this endeavor, such as linking volumes to the complexities of decoding information within the black hole, and several explicit calculations have been developed to demonstrate this duality [5–21].

Quantum complexity is a measure of least steps to complete a task by applying gates only from a set of finite simple operations. The ambiguity in determining the exact value of complexity arises from the arbitrariness of the choice of gate set and the cost assigned to each gate. It was argued that, instead of a shortcoming, this ambiguity connects nicely with the ambiguity of rescaling freedom of the length/volume in its holographic dual [8, 9]. The scaling of the complexity with the size of the problem is a robust property, and the quantum circuit complexity is shown to grow linearly with the number of Haar-random two-qubit quantum gates [22].

Inspired by the ER=EPR proposal [23], the observation of linear growth of the worm-hole length and the switchback effect of external perturbations, the quantum complexity is conjectured to be dual to volume of the codimension-one maximal slice (Complexity-Volume proposal, or CV) [5, 6], gravitational action in the Wheeler-DeWitt patch (Complexity-Action proposal, or CA) [24–26] and the spacetime volume of the Wheeler-DeWitt patch (Complexity-Volume proposal 2.0, or CV2.0) [7]. In the CV conjecture, the holographic complexity is conjectured to be dual to the maximal volume of the hypersurface anchored at the boundary CFT slice Σ_{CFT} , viz.

$$C_V(\Sigma_{\text{CFT}}) = \max_{\partial\mathcal{B}=\Sigma_{\text{CFT}}} \left[\frac{\mathcal{V}(\mathcal{B})}{G_N \ell_{\text{bulk}}} \right], \quad (1.1)$$

where \mathcal{B} is the bulk hypersurface. The CA conjecture offers an alternative to the CV proposal and states that the complexity is represented by the integral of the gravitational action in the Wheeler-DeWitt patch, which is defined as the domain of dependence of the slice \mathcal{B} . It is expressed as:

$$C_A(\Sigma_{\text{CFT}}) = \frac{I_{\text{WDW}}}{\pi \hbar}. \quad (1.2)$$

The CA proposal was investigated in various models. See Refs. [27–35] for a non-exhaustive list of works. The CV2.0 proposal combines the CV and CA conjectures and proposes that the complexity is simply given by the spacetime volume of the Wheeler-DeWitt patch anchored at the given boundary states,

$$C_{V2}(\Sigma_{\text{CFT}}) = \frac{V_{\text{WDW}}}{G_N \ell_{\text{bulk}}^2}. \quad (1.3)$$

Recently, it was realized that the dual of holographic complexity, which exhibits linear growth and the switchback effect at late times, can be extended to an infinite family of observables of either codimension zero or one [8, 9, 36]. For codimension-one observables, which is the focus of this paper, the generalized volume is given by

$$C_{\text{gen}}(\tau) = \max_{\partial\Sigma(\tau)=\Sigma_{\text{CFT}}} \left(\frac{1}{G_N L} \int_{\Sigma(F_2)} d^{D-1} \sigma \sqrt{h} F_1(g_{\mu\nu}; X^\mu(\sigma)) \right), \quad (1.4)$$

where the slice $\Sigma(F_2)$ is the extremal surface for a scalar function F_2 and τ is the boundary time. Notably, F_2 can be any scalar function, and it is not required to be the same as F_1 in the integrand. It is shown that at the late times, different choices of the functions F_2 result in the same late-time behavior for the generalized volume [8]. Therefore, demonstrating the simpler case $F_1 = F_2$ should suffice for the discussion. The proposal of Complexity=Anything (CAny) is useful for probing the singularities of black holes by tuning the coupling parameters [9, 36]. Recent development extends the CAny to de-Sitter spaces [37], charged black holes [10, 38], and two-sided Holographic Violating black branes [39]. The details of this proposal will be delineated in the subsequent sections.

The goal of this paper is to explore the generalized CAny proposal of the codimension-one surfaces for Gauss-Bonnet black holes in four dimensions and higher. We show that in

four dimensions, the effective potentials for the Gauss-Bonnet black holes, which dictate the time evolution of the extremal surfaces, are qualitatively different from those in higher dimensions due to the existence of multiple horizons. This feature in 4D Gauss-Bonnet black holes guarantees the linear growth of the generalized volume at late times, regardless of the chosen coupling parameters. This trait of universal linear growth is absent for Gauss-Bonnet black holes in dimensions higher than four. In addition, we explore the scenario when multiple extremal surfaces exist and show that different rates of volume growth can be assigned to the surfaces. We demonstrate the time evolution of conserved momenta corresponding to different configurations of the extremal surfaces and illustrate the conditions for the generalized volume to be qualified as the dual of the holographic complexity. In Sec. 2, we provide background information on the essential features of Gauss-Bonnet black holes. In Sec. 3, we review the CAny proposal and illustrate its application to codimension-one observables. In Sec. 4, we concentrate on the CAny proposal in 4D Gauss-Bonnet gravity. The analysis of 5D Gauss-Bonnet gravity is provided in Sec. 5. We summarize our results in the last section.

2 Gauss-Bonnet-AdS black holes

The Gauss-Bonnet Lagrangian is a natural generalization of general relativity which modifies the equations of motion in dimensions larger than four. In 4D, the Gauss-Bonnet term is topological and does not contribute to the equations. Several techniques have been developed to establish a consistent nontrivial 4D Gauss-Bonnet gravity, and the related issues have triggered vigorous discussions [40]. Though issues in 4D are more subtle and not entirely understood, it is still worthwhile to explore the full consequences of the theory.

The 4D Gauss-Bonnet-AdS black holes have two horizons, which implies that the central singularity is time-like [41–43]. In spacetime dimensions $D \geq 5$, the solution has only one horizon, similar to the Schwarzschild solution.. The topology of Gauss-Bonnet black holes is an active research topic and has been investigated in Refs. [44–48]. The action for the GB-AdS black hole is given by [49]

$$\mathcal{S} = \frac{1}{16\pi} \int d^D x \sqrt{-g} (R - 2\Lambda + \tilde{\alpha} \mathcal{L}_{GB}), \quad (2.1)$$

where $\mathcal{L}_{GB} = R^2 - 4R_{\mu\nu}R^{\mu\nu} + R_{\mu\nu\rho\sigma}R^{\mu\nu\rho\sigma}$ and $\Lambda = -\frac{(D-1)(D-2)}{2L^2}$. For simplicity, we denote $\alpha = \tilde{\alpha}(D-3)(D-4)$. Note that the GB coupling $\tilde{\alpha}$ is scaled as $\frac{1}{D-4}$ which cancels out the $(D-4)$ factor in the definition of α . Taking the limit as $D \rightarrow 4$ yields the effective equation of the Einstein-Gauss-Bonnet-AdS model in 4D. The causality bound from the boundary CFT requires $|\alpha/L^2| \ll 1$ [50]. On the other hand, a well-defined vacuum of the theory also requires that $0 \leq \frac{4\alpha}{L^2} \leq 1$. For spherically symmetric solution, the metric is given by

$$ds^2 = -f(r)dt^2 + f(r)^{-1}dr^2 + r^2 d\Omega_{D-2}^2, \quad (2.2)$$

$$(2.3)$$

where Ω_{D-2} is the phase-space volume of the $(D-2)$ -dimensional sphere. In Eddington-Finkelstein coordinates, it reads

$$ds^2 = -f(r)dv^2 + 2dvdr + r^2 d\Omega_{D-2}^2, \quad (2.4)$$

where the infalling coordinate $v = t + r_*(r)$ with $r_*(r) = -\int_r^\infty \frac{dr'}{f(r')}$, and the lapse function $f(r)$ is given by

$$f(r) = 1 + \frac{r^2}{2\alpha} \left[1 - \sqrt{1 + 4\alpha \left(\frac{w}{r^{D-1}} - \frac{1}{L^2} \right)} \right]. \quad (2.5)$$

Here, $w = 16\pi GM / ((D-2)\Omega_{D-2})$ is the re-scaled mass of the black hole. The location of the horizon satisfies $f(r_h) = 0$, viz.,

$$w = r_h^{D-3} \left(1 + \frac{r_h^2}{L^2} + \frac{\alpha}{r_h^2} \right). \quad (2.6)$$

The temperature of the black hole is given by

$$T_{BH} = \frac{f(r)'}{4\pi} \Big|_{r=r_h} = \frac{(D-3)r_h^2 + (D-1)r_h^4/L^2 + (D-5)\alpha}{4\pi r_h (r_h^2 + 2\alpha)}. \quad (2.7)$$

3 CAny

For the codimension-one observable, CAny generalizes the CV and the CA proposals to observables of the form

$$C_{gen}(\tau) = \max_{\partial\Sigma(\tau)=\Sigma_{CFT}} \left(\frac{1}{G_N L} \int_{\Sigma} d^{D-1}\sigma \sqrt{h} F_1(g_{\mu\nu}; X^\mu(\sigma)) \right), \quad (3.1)$$

where the slice Σ is the extremal surface for the scalar function F_2 which is not necessarily the same as the scalar function F_1 in the integrand and τ is the boundary CFT time with $\tau = 2t_L = 2t_R$. The codimension-one extremal slice can be readily extended to the codimension-zero case, where the integration spans the spacetime region enclosed by two extremal slices, along with the contributions from the two codimension-one slices. These observables exhibit linear growth with time at late times and display the switchback effect. In this study, we investigate the CAny conjecture in Gauss-Bonnet gravity and discuss the conditions under which this conjecture holds.

For simplicity, we pick $F_1 = F_2$ and consider the spherically symmetric scalar functions. Choosing the parameterization $(v(\sigma), r(\sigma), \vec{\Omega})$, we have

$$C_{gen}(\tau) = \frac{\Omega_{D-2}}{G_N L} \int_{\Sigma} d\sigma \sqrt{-f(r)\dot{v}^2 + 2\dot{v}\dot{r}} F_1(r). \quad (3.2)$$

Note that by choosing $F_1 = 1$, it returns to the CV proposal. One can identify the generalized complexity as the action and the integrand as the Lagrangian. From the classical equation of motion $\frac{\partial S}{\partial q^i} = \frac{\partial L}{\partial \dot{q}^i} \Big|_{\partial\Sigma}$, we obtain

$$\frac{dC_{gen}}{d\tau} = \frac{1}{2} \frac{\partial(\sqrt{h}F_1)}{\partial \dot{t}} \Big|_{\partial\Sigma(\tau)} = \frac{1}{2} P_t \Big|_{\partial\Sigma(\tau)}. \quad (3.3)$$

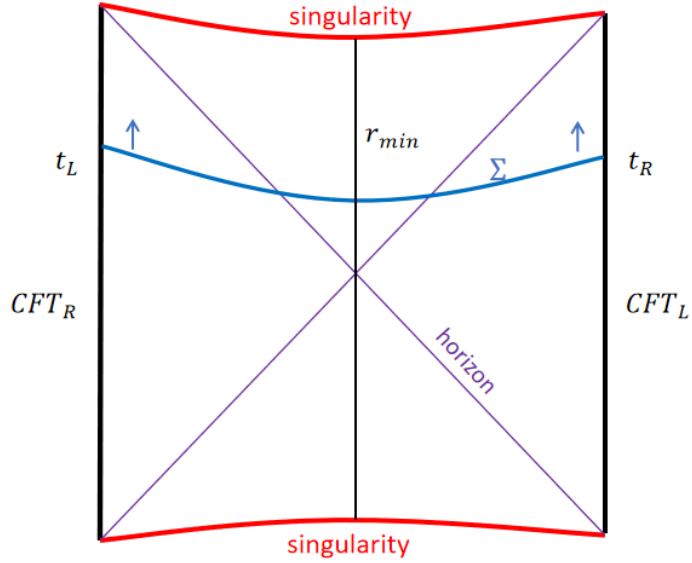


Figure 1. Extremal slices

The generalized complexity is diffeomorphism invariant and we employ our freedom of reparametrization to pick the gauge condition

$$\sqrt{-f(r)\dot{v}^2 + 2\dot{v}\dot{r}} = F_1(r) \left(\frac{r}{L}\right)^{D-2}. \quad (3.4)$$

The momentum P_ν conjugate to the infalling time ν is

$$P_\nu = \frac{\partial \mathcal{L}}{\partial \dot{\nu}} = \dot{r} - f(r)\dot{\nu}, \quad (3.5)$$

where the dots are the derivatives taken with respect to the parameter σ which increases from the left AdS boundary to the right AdS boundary. The above two equations give the extremality conditions:

$$\dot{r} = \pm \sqrt{P_\nu^2 + f(r)F_1^2 \left(\frac{r}{L}\right)^{2(D-2)}}, \quad (3.6)$$

$$\dot{\nu} = \frac{1}{f(r)} \left(-P_\nu \pm \sqrt{P_\nu^2 + f(r)F_1^2 \left(\frac{r}{L}\right)^{2(D-2)}} \right) = \frac{1}{f(r)} (-P_\nu + \dot{r}). \quad (3.7)$$

Comparing the equations with the motion of a classical particle, we obtain the equations of motion

$$\dot{r}^2 + \tilde{U}(r) = P_\nu^2 \quad \text{with} \quad \tilde{U}(r) = -f(r)F_1(r)^2 \left(\frac{r}{L}\right)^{2(D-2)}. \quad (3.8)$$

Note that

$$\dot{\nu} = \dot{t} + \frac{dr_*}{dr} \frac{dr}{d\sigma} = \dot{t} + \frac{\dot{r}}{f(r)}, \quad (3.9)$$

and the conjugate momentum P_ν is conserved for a specific boundary time τ . Combining it with the above extremality condition Eq. (3.7), we have

$$\dot{t} = -\frac{P_\nu}{f(r)}. \quad (3.10)$$

From the equations of \dot{t} and $\tilde{U}(r)$, we can recast the generalized volume as

$$C_{gen}(\tau) = \frac{\Omega_{D-2}}{G_N L} \int_\Sigma dt \frac{\tilde{U}(r(t))}{P_\nu}. \quad (3.11)$$

Here the integration is taken on the extremal surface so that P_ν in the denominator is a constant. The boundary time τ is related to the conjugate momentum by

$$t = \tau/2 = - \int_{r_{\min}}^\infty dr \frac{P_\nu}{f(r) \sqrt{P_\nu^2 - \tilde{U}(r)}}, \quad (3.12)$$

where r_{\min} is the minimal radius lying on the timelike surface $t = 0$. The growth rate of the complexity

$$\frac{dC_{gen}}{d\tau} = \frac{\Omega_{D-2}}{G_N L} P_\nu(\tau) \quad (3.13)$$

can be calculated from the effective potential. The linear growth of C_{gen} at late times is dedicated by the condition that $\lim_{\tau \rightarrow \infty} P_\nu(\tau) := P_\infty$ is constant and the effective potential $\tilde{U}(r)$ has a local maximum inside the horizon. In this case,

$$\lim_{\tau \rightarrow \infty} \frac{dC_{gen}}{d\tau} = \frac{\Omega_{D-2}}{G_N L} P_\infty = \frac{\Omega_{D-2}}{G_N L} \sqrt{\tilde{U}(r_f)}, \quad (3.14)$$

where $r = r_f$ is the radius of the local maximum. In certain parameter regimes, the effective potential may have more than one local maxima as shown in Fig. 2.

4 Codimension-one extremal slices for Gauss-Bonnet in 4D

4.1 Existence of local maxima

For Gauss-Bonnet black hole, one simplest extension beyond the CV proposal in CAny is to add a higher curvature terms such as the square of Weyl tensors

$$C^2 = \frac{2}{D(D-1)} R^2 - \frac{4}{D-1} R_{\mu\nu} R^{\mu\nu} + R_{\mu\nu\rho\sigma} R^{\mu\nu\rho\sigma}. \quad (4.1)$$

The analysis is much simplified in 4D due to the different topology of Gauss-Bonnet-AdS black holes. For spherically symmetric solutions of Gauss-Bonnet black holes in 4D, the square of Weyl tensor is given by

$$C^2(r) = \frac{12L^2 w^2 (L^2 (r^3 + \alpha w) - 4\alpha r^3)^2}{(L^2 (r^4 + 4\alpha r w) - 4\alpha r^4)^3}. \quad (4.2)$$

One straightforward generalization of the CV proposal (which is recovered by setting $F_1 = 1$) is to pick $F_1(r) = 1 + \lambda L^4 C^2(r)$. This scalar function is the simplest nontrivial function in Einstein gravity in vacuum and is the most studied one. The same function is chosen for comparison with existing results.¹ Then, the generalized holographic complexity is defined as the integration of the scalar function on the space volume that extremizes the integral, viz.,

$$C_{gen}(\tau) = \frac{\Omega_{D-2}}{G_N L} \int_{\Sigma} d\sigma \sqrt{-f(r)\dot{v}^2 + 2\dot{v}\dot{r}} (1 + \tilde{\lambda} L^4 C^2(r)). \quad (4.3)$$

To ensure that the late time evolution of the generalized complexity increases linearly with the boundary time τ , we plot the effective potential $\tilde{U}(r)$ as a function of radius r . For a reminder, the effective potential reads,

$$\tilde{U}(r) = -f(r)F_1(r)^2 \left(\frac{r}{L}\right)^{2(D-2)} = -f(r) (1 + \lambda L^4 C^2(r))^2 \left(\frac{r}{L}\right)^{2(D-2)}. \quad (4.4)$$

The Penrose diagram of a Gauss-Bonnet-AdS black hole in 4D is similar to that of a charged black hole in that they are both equipped with two horizons. For spacetime regions inside the inner horizon or outside the outer horizon, i.e., $r < r_-$ or $r > r_+$, the lapse function is positive $f(r) > 0$. For spacetime regions between the two horizons, $f(r) < 0$. Therefore, the effective potential $\tilde{U}(r)$ is positive between the horizons and negative otherwise as shown in Fig. 2. This ensures that the effective potential always has the local maximum $\tilde{U}(r_f)$ inside the horizon, which is the condition for the linear growth of complexity at late times. We will elaborate on this point further in the following discussion.

To see that any such observables in $D = 4$ suffice as candidates for holographic complexity, we show that $\lim_{\tau \rightarrow \infty} P_\nu(\tau) = P_\infty$ is constant. Recall that the boundary time is

$$\tau = -2 \int_{r_{min}}^{\infty} dr \frac{P_\nu}{f(r) \sqrt{P_\nu^2 - \tilde{U}(r)}}, \quad (4.5)$$

where r_{min} is determined by $P_\nu^2 - \tilde{U}(r_{min}) = 0$. The lapse function $f(r)$ is continuous and nonzero between the two horizons. For $P_\nu^2 < \tilde{U}(r_f)$ where r_f is the radius of the local maximum of the effective potential, $\tilde{U}(r) \simeq P_\nu^2 + \tilde{U}'(r_{min})(r - r_{min})$ in the vicinity of $r = r_{min}$. The integrand $\frac{P_\nu}{f(r) \sqrt{P_\nu^2 - \tilde{U}(r)}}$ of Eq. (4.5) is regular everywhere except at $r = r_{min}$. Notice that for $U'(r_{min}) \neq 0$, one can take the Cauchy principal value and the integral which gives the boundary time τ is finite. At late times, $\tau \rightarrow \infty$, and it corresponds to $P_\nu^2 \rightarrow \tilde{U}(r_f)$. In this case, $\tilde{U}(r) \simeq P_\nu^2 + \frac{1}{2}\tilde{U}''(r_f)(r - r_f)^2 + O(r - r_f)^3$ near the local maximum $r = r_f$. One can see that as long as $r = r_f$ is the local maximum for $\tilde{U}(r)$, the function in the integrand is no longer integrable in the domain. In other words, the integral is divergent with the irregular point at $r = r_f$. This suggests that when P_ν approaches $\tilde{U}(r_f)$, the result of the integral which gives τ can take arbitrarily large values. Therefore,

¹The simpler choices of scalar functions such as R^2 and $R_{\mu\nu}R^{\mu\nu}$ do not contribute in the vacuum solutions of the Einstein gravity, therefore are not of particular interest in related studies.

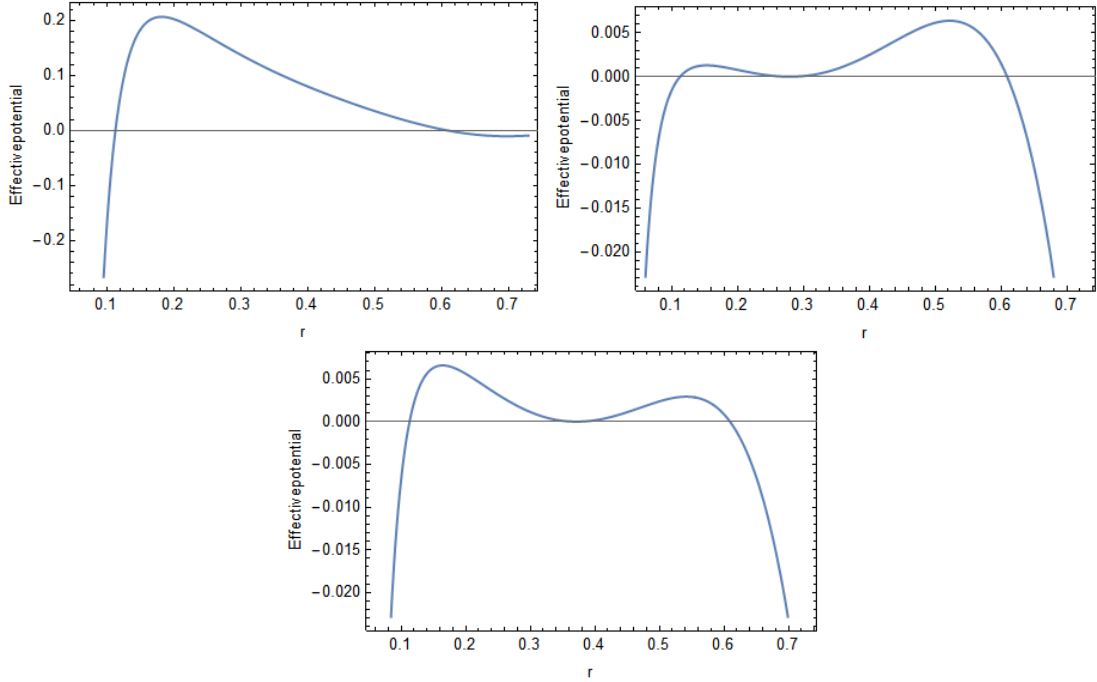


Figure 2. Effective potential $\tilde{U}(r)$ as a function of radius r in 4D. Left: $\lambda = -0.1$. Right: $\lambda = -0.01$. Bottom: $\lambda = -0.02$. $\tilde{U}(r)$ vanishes on the inner and outer horizons and stays positive between them. This feature of the effective potential is universal in 4D Gauss-Bonnet black holes. For all, $L = w = 1$, $\alpha = 0.1$.

at late times $\tau \rightarrow \infty$, the conjugate momentum P_ν approaches a constant $P_\nu^2 \rightarrow \tilde{U}(r_f)$, and the growth rate of the complexity is

$$\lim_{\tau \rightarrow \infty} \frac{dC_{gen}}{d\tau} = \frac{\Omega_{D-2}}{G_N L} \sqrt{\tilde{U}(r_f)}. \quad (4.6)$$

Therefore, Any proposal has the natural realization at $D = 4$ in Gauss-Bonnet-AdS black holes. No additional constraints or regularization for the scalar field is required.

4.2 Dipping and non-Dipping branches

In the case of 4D Gauss-Bonnet-AdS black holes, the extremal surface can not approach arbitrarily close to the singularity for arbitrarily large conjugate momenta as it does for planar black holes in Einstein’s theory [9]. The effective potentials in Ref. [9] diverge to infinity as $r \rightarrow 0$, and that the equation $P_\nu^2 = \tilde{U}$ always has a solution for arbitrarily large conjugate momentum P_ν . In contrast, the effective potential for a 4D Gauss-Bonnet-AdS black hole [see Fig. 2] is similar to that of RN-AdS black holes, where the effective potential approaches negative infinity as $r \rightarrow 0$ [10]. The “dipping branch” in this scenario corresponds to the time evolution of P_ν approaching P_∞ from above, i.e., P_ν decreases with the boundary time τ which is given by

$$\tau = -2 \int_{r_{\min}}^{r_{\max}} dr \frac{P_\nu}{f(r) \sqrt{P_\nu^2 - \tilde{U}(r)}}, \quad (4.7)$$

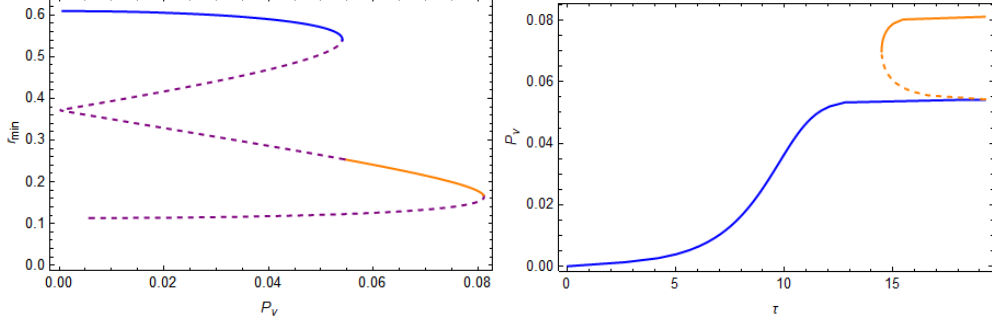


Figure 3. Conserved momentum when effective potential has two local maxima with global maximum locates inside. Left: the minimal radius r_{\min} of the extremal surface vs conserved momentum at $\lambda = -0.02$. The dashed curves correspond to the hypersurfaces that do not have boundaries at Σ_{CFT} . Right: boundary time vs conserved momentum at $\lambda = -0.02$. The dashed lines correspond to the hypersurface where P_ν decreases and r_{\min} increases as time evolves. The generalized volume evaluated on this slice is smaller than its counterpart measured along the blue curve. For both, $L = w = 1$, $\alpha = 0.1$.

where r_{\min} the solution of $P_\nu = \tilde{U}(r)$. This process is represented by the orange solid lines in Fig. 3 (a) going from right to left and also by the dashed orange branch in Fig. 3 (b). One can compute numerically that the transitioning point from no dipping branch to the emergence of a dipping branch occurs at $\lambda \simeq -0.05$. It is worthwhile to point out that the extremal surfaces corresponding to the dipping branches in both the 4D Gauss-Bonnet gravity and the planar Einstein gravity do not yield the maximal holographic complexity at late times. This can be seen by comparing the late-time generalized volume evaluated on the dipping branch with that on the non-dipping branch

$$\lim_{\tau \rightarrow \infty} (C_{\text{no-dip}}(\tau) - C_{\text{dip}}(\tau)) = \lim_{\tau \rightarrow \infty} \frac{\Omega_{D-2}}{G_N L} \int_{t=0}^{t=\tau} dt \left(P_\infty - \frac{\tilde{U}(r(t))}{P_\infty} \right). \quad (4.8)$$

At late times, as $P_\nu(\tau) \rightarrow P_\infty$ and the $\tilde{U}(r(t)) \leq P_\infty^2$, the right-hand side of the above equation remains positive. Therefore, we can draw the following conclusion: *the surface yielding the maximal complexity is always the one whose minimal radius approaches the local maximum of the effective potential.*

4.3 Phase transition of the extremal slice

One feature of the holographic complexity in 4D Gauss-Bonnet-AdS black holes is the appearance of multiple local maxima in the effective potential as illustrated in Fig. 2 (b) and (c). Consequently, the late-time behavior of the generalized volume is now characterized by two different branches, resulting in different rates of increase for the generalized volume-complexity.

Notably, there is no continuous variation from one branch to the other along the trajectory of equations of motion. The time evolution of the conserved momentum P_ν with respect to the boundary time τ extends to an infinite future, ultimately approaching $P_{\infty,R}$, which is the asymptotic conserved momentum defined through Eq. (4.5) as $\tau \rightarrow \infty$. It is

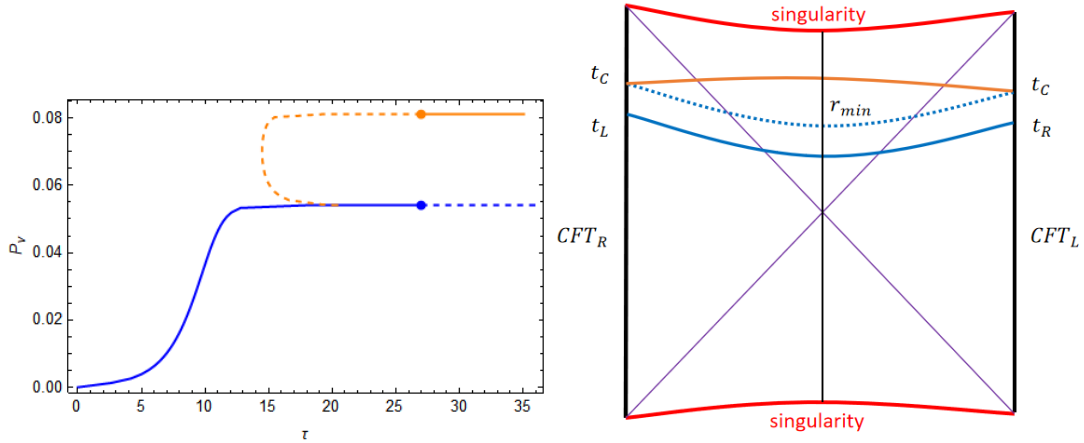


Figure 4. Coexistence of two branches of extremal surfaces at $\lambda = -0.02$. Left: the boundary time τ vs the conserved momentum P_ν . The two colors represent the two branches of the extremal surfaces. The blue curve represents the evolution from $(0, 0)$. The generalized volume-complexity along the blue curve, which is proportional to the area below the curves, is dominating at the beginning of coexistence of two branches. After some critical time t_C , the volume-complexity computed from the orange curve dominates, and the conserved momentum jumps to a higher value discontinuous. Right: the Penrose diagram of the process. For both, $L = w = 1$, $\alpha = 0.1$.

the value of P_ν at the right peak of the effective potential and is represented by the end value of the blue curve in Fig. 4 (a). Along the trajectory of equations of motion, the evolution of the generalized volume-complexity is determined either by the left or by the right local maximum of the effective potential. Both trajectories of P_ν are smooth.

However, according to the volume-complexity conjectures, the generalized volume-complexity C_{gen} is determined by the maximum value obtained across all the branches. This requirement results in discontinuous jumps of the extremal surface from the blue curve to the orange one closer to the singularity at time t_C as shown in Fig. 4. We remind that this “phase transition” is not describable by the equations of motion of the extremal surfaces (Eq. 3.7) but rather is from the definition of the volume-complexity

$$C_{gen} = \max_{\Sigma} \left(\frac{\Omega_{D-2}}{G_N L} \int_{\Sigma} P_\nu(\tau) d\tau \right), \quad (4.9)$$

where Σ ’s are the extremal surfaces.

In Fig. 4 (b), we demonstrate the two extremal surfaces in the Penrose diagram. At the critical time t_C , the volume-complexity evaluated on the two surfaces is identical. However, after the critical time, the surface closer to the singularity [the solid orange curve] exhibits a larger volume-complexity. As shown in Fig. 3 (a), the non-dipping branch, represented by the blue solid line on the top, has a lower generalized volume at $\tau \rightarrow \infty$. The extremal surface that generates the largest volume complexity jumps to the one ending at the left peak of Fig. 2(c), and is represented by the orange solid line in Figs. 3 and 4. This behavior resembles a phase transition and was briefly discussed in [10]. In particular, depending on the shape of the effective potential and in higher dimensional cases, this phase transition

between different branches of $P_\nu - \tau$ diagrams can occur more than once. Overall, *the late-time behavior is always dictated by the maximal peak of the effective potential $\tilde{U}(r)$ and the extremal surface after the transition always moves closer to the singularity.*

5 Codimension-one extremal slices for Gauss-Bonnet in 5D

In contrast to the four-dimensional case, Gauss-Bonnet black holes of dimensions higher than five exhibit the presence of only one horizon. For $d > 4$, the analysis is similar and can be easily generalized, but it becomes much more complicated from Weyl tensor terms. Therefore, in this study, we will explicitly illustrate the five-dimensional case to demonstrate the constraints on the coupling parameter necessary for the existence of the extremal surface at late times.

5.1 Existence of local maxima

In 5D, the black hole has a minimal black hole mass condition, namely, $w > \alpha$. It possesses a single horizon, and its corresponding effective potential does not automatically admit a local maximum inside the horizon as observed in the 4D case. Notably, the lapse function $f(r) < 0$ for the inside of the black hole $r < r_h$, which leads to the effective potential being positive inside the horizon, i.e., $\tilde{U}(r) > 0$. Since $\tilde{U}(r) < 0$ for $r > r_h$, it does not automatically ensure the existence of the local maximum as that in 4D. Therefore, the volume-complexity does not have the same simple universality as in 4D.

For the spherically symmetric solutions of Gauss-Bonnet black holes in 5D, the square of Weyl tensor is

$$C^2(r) = \frac{8L^2w^2 (L^2 (3r^4 + 4\alpha w) - 12\alpha r^4)^2}{r^4 (L^2 (r^4 + 4\alpha w) - 4\alpha r^4)^3}. \quad (5.1)$$

Therefore, the effective potential reads

$$\tilde{U}(r) = -f(r) \left(1 + \lambda \frac{8L^6w^2 (L^2 (3r^4 + 4\alpha w) - 12\alpha r^4)^2}{r^4 (L^2 (r^4 + 4\alpha w) - 4\alpha r^4)^3} \right)^2 \left(\frac{r}{L} \right)^6. \quad (5.2)$$

In this case, it is difficult to directly solve for the local maximum of $\tilde{U}(r)$. Nevertheless, one may notice that the effective potential $\tilde{U}(r) \rightarrow \infty$ as $r \rightarrow 0$ as illustrated in Fig. 5. The future null slice which hugs the singularity will always be the global maximum when evaluating the integral. This point will be delineated in detail later.

For $\lambda < 0$, we now show that the extremal surface always exists if the coupling parameter λ lies within the range $\lambda_c < \lambda < 0$ where λ_c is the critical coupling to be determined later. For $\lambda < 0$, $\lambda C^2(r) \rightarrow -\infty$ near the singularity. Since $C^2(r) \rightarrow 0$ as $r \rightarrow \infty$, one can see that $\tilde{U}(r)/f(r) = 0$ always has roots. For simplicity, we rewrite the square of Weyl tensor as

$$C^2(\mathcal{R}) \propto \frac{(3\mathcal{R} + \beta)^2}{\mathcal{R}(\mathcal{R} + \beta)^3}, \quad (5.3)$$

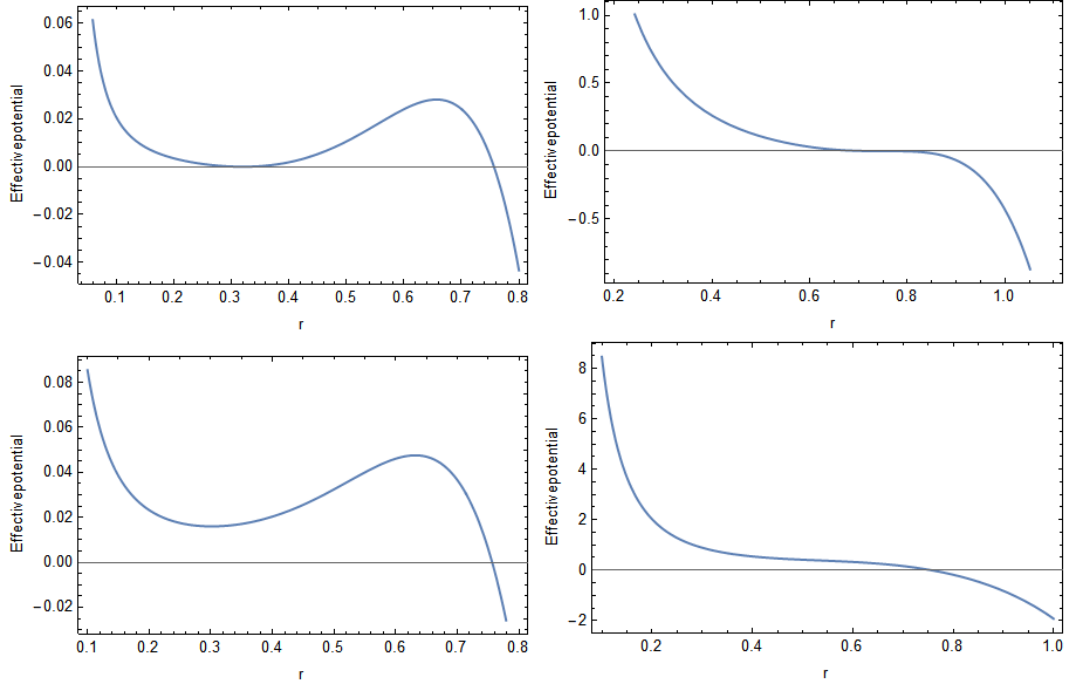


Figure 5. Effective potential $\tilde{U}(r)$ as a function of radius r in 5D. (a) $\lambda = -0.0005 > \lambda_c$. This corresponds to the existence of the local maximum inside the horizon. (b) $\lambda = -0.008877 = \lambda_c$. This demonstrates the effective potential at exactly the critical point when the local maximum approaches the horizon and disappears. (c) $\lambda = 0.001 < \lambda'_c$. (d) $\lambda = 0.01 > \lambda'_c$. For all, $L = w = 1$, $\alpha = 0.1$. Unlike the case in 4D, $\tilde{U}(r) \rightarrow \infty$ close to the singularity $r \rightarrow 0$.

where $\mathcal{R} = (L^2 - 4\alpha)r^4$ and $\beta = 4\alpha w L^2$. We remind that $(L^2 - 4\alpha) > 0$ is required by the well-defined vacuum in the theory. One can check from the above formula Eq. (5.3) that $dC^2(\mathcal{R})/d\mathcal{R} < 0$ holds for all $\mathcal{R} > 0$. Therefore, the equation for the effective potential

$$\tilde{U}(r) = -f(r)(1 + \lambda C^2(r))^2 (r/L)^{2(D-2)} = 0 \quad (5.4)$$

has roots inside the horizon when the coupling parameter satisfies $\lambda_c < \lambda < 0$, where λ_c is the critical value of λ that is determined by $\lambda_c C^2(r_h) = -1$ where r_h is the radius of the horizon. The case $\lambda = \lambda_c$ corresponds to when the local minimal of the effective potential is zero at the horizon. Obviously, for $\lambda < \lambda_c$, the effective potential $\tilde{U}(r) > 0$ for $r < r_h$ and it does not have a root inside the horizon. The effective potential $\tilde{U}(r)$ monotonically decreases inside the horizon, therefore, in this case it does not have a local maximum. In conclusion, the above analysis proves that when $\lambda_c < \lambda < 0$, the requirement of linear growth for the observable C_{gen} at late times is satisfied. In addition, the analysis also holds for Gauss-Bonnet black holes of higher-dimensions.

For $\lambda \geq 0$, the effective potential satisfies $\tilde{U}(r) > 0$ for $r < r_h$ so that it does not have a root inside the horizon. We notice that the effective potential $\tilde{U}(r) \propto -f(r)r^6(1 + \lambda C^2(r))^2$.

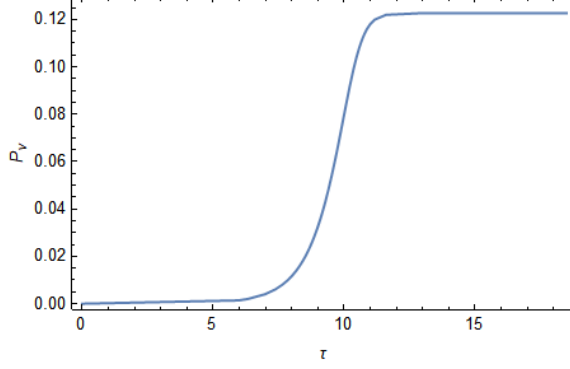


Figure 6. The change of conjugate momentum P_ν with boundary time τ . $\lambda = -0.002$, $L = w = 1$, and $\alpha = 0.1$.

For $r^2 \ll \alpha$ (near the singularity), one has

$$\begin{aligned} \frac{d(-f(r)r^6)}{dr^4} &= \frac{-2r^4 \left(\sqrt{-\frac{4\alpha}{L^2} + \frac{4\alpha w}{r^4} + 1} - 1 \right) - 3\alpha\sqrt{r^4} \sqrt{-\frac{4\alpha}{L^2} + \frac{4\alpha w}{r^4} + 1} + 6\alpha w - \frac{8\alpha r^4}{L^2}}{2\alpha\sqrt{-\frac{4\alpha}{L^2} + \frac{4\alpha w}{r^4} + 1}} \\ &\simeq \frac{3\alpha w - 3\alpha\sqrt{\alpha w}}{\alpha\sqrt{4\alpha w}} r^2 > 0. \end{aligned} \quad (5.5)$$

Both the effective potential and its derivative with respect to the radius r are positive inside the horizon and $\tilde{U}(r_h) = 0$ on the horizon. This guarantees that when $\lambda = 0$ there exists a local maximum $\tilde{U}(r)$ inside the horizon. Since the square of Weyl tensor $C^2(r)$ is a monotonically decaying function, it follows that there exists a maximal value of $\lambda'_c \geq 0$ such that:

- (1) for $0 \leq \lambda < \lambda'_c$, the effective $\tilde{U}(r)$ has a local maximum inside the horizon;
- (2) for $\lambda > \lambda'_c$, $d\tilde{U}(r)/dr < 0$ inside the horizon.

This completes the existence proof of the desired shape of the effective potential within a finite range of the coupling parameter. The maximal value λ'_c depends non-trivially on w, α, L and can be determined numerically. The graphic illustration of the above results is shown in Fig. 5. Combining the analysis above, we conclude that C_{gen} is a well-behaved observable for the holographic complexity as long as $\lambda_c < \lambda < \lambda'_c$ where $\lambda_c = -1/C^2(r_h) < 0$ and $\lambda'_c > 0$.

As shown in Fig. 6, when the coupling parameter is within the above-mentioned range, the conserved momentum monotonically increases with time and approaches a finite asymptotic value P_∞ . In this case, the generalized volume-complexity has a constant rate of increase at late times as $\lim_{\tau \rightarrow \infty} \frac{dC_{gen}}{d\tau} = \frac{\Omega_{D-2}}{G_N L} P_\infty$.

5.2 Couplings outside the allowed range

In the previous section, we demonstrated that the desired behaviors of the volume-complexity observable only manifest within a finite range of coupling parameters. This stands in contrast to the 4D case where no such constraints are necessary. However, even for the

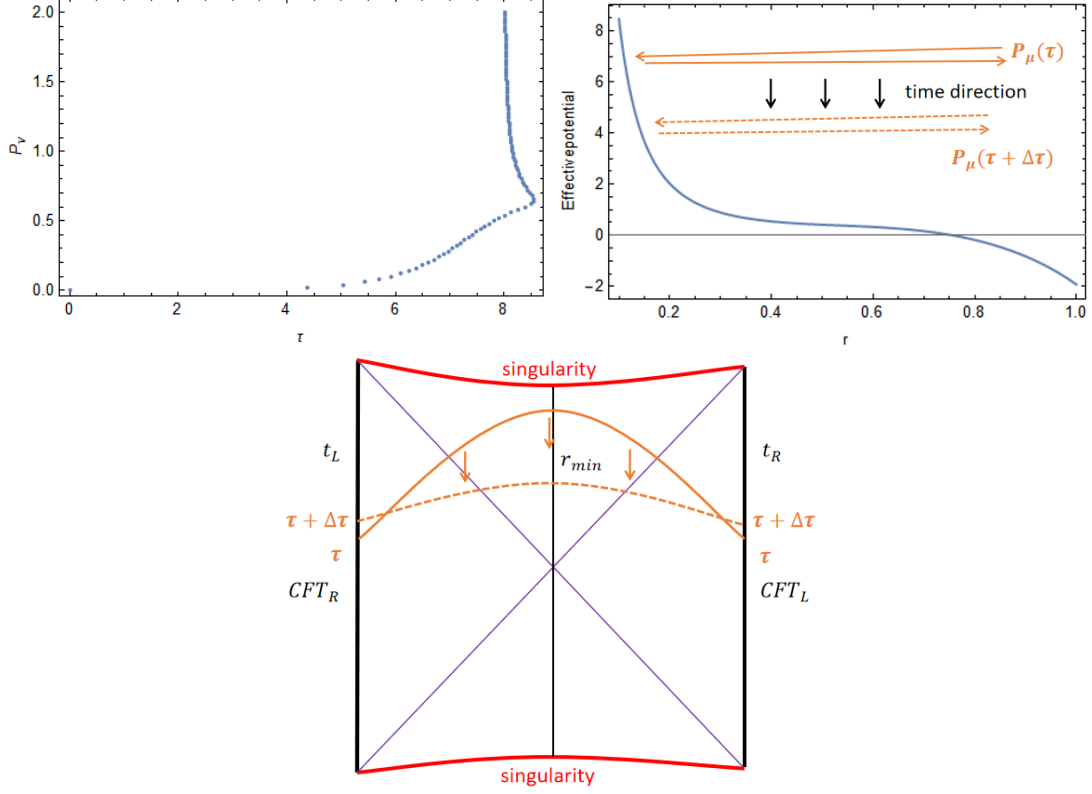


Figure 7. (a) Time evolution of the conserved momentum with $\lambda = 0.01$, $L = w = 1$, and $\alpha = 0.1$. (b) Diagrammatic illustration of the evolution of the conserved momentum at large values in (a). (c) The Penrose diagram for the process in (b). The parameters are $L = w = 1$, $\alpha = 0.1$ and $\lambda = -0.01$.

coupling parameters outside the desired range, we can just as well explore the behaviors of the conserved momentum and the extremal surfaces.

First of all, we examine the evolution of the conserved momentum using Eq. (4.5). For instance, consider a coupling parameter like $\lambda = 0.01$, which exceeds the critical value λ'_c . As depicted in Fig. 5 (d), in this scenario, the effective potential monotonically decreases. We evolve the extremal surface from $\tau = 0$ and $P_\nu = 0$. As shown in Fig. 7 (a), the evolution of the conserved momentum lasts only for a finite time before the extremal surface ceases to exist. On the other hand, if we start with an extremely large P_ν , which corresponds to the extremal surface extending arbitrarily close to the singularity, P_ν rapidly decays to its final value and thereafter, no solutions exist any longer. This case is diagrammatically represented in Fig. 7 (b). In Fig. 7 (c), we depict the corresponding changes of the extremal surface in the Penrose diagram. Beginning with the extremal surface extending close to the singularity, the slice rapidly deforms into the one that is further away from the singularity before ceasing to exist. In this case, the generalized volume does not have a dual quantum complexity at late times.

6 Discussion

In the above analysis, the correction to the boundary time due to the presence of Gauss-Bonnet couplings is not considered [12]. In general, for a more physical choice of boundary time that has the speed of light equal to one, the time coordinate should be shifted according to $t \rightarrow \frac{1}{N}t$ where $N = \sqrt{\frac{1}{2} \left(1 + \sqrt{1 - 4\alpha/L^2} \right)}$. Therefore, the rate of change in complexity $\frac{dC}{dt}$ is modified by a constant multiplicative factor N . The Gauss-Bonnet correction to the boundary time decreases the complexity rate by a constant factor, but it does not affect our discussion.

In the Complexity=Anything conjecture, a much wider class of observables is considered as viable candidates for the dual of holographic complexity. The core of evaluating the generalized volume, which is the complexity dual, is to find the extremal slice. In this study, we explored the CAny conjecture in four- and five-dimensional Gauss-Bonnet gravity in anti-de Sitter space. Specifically, we demonstrated the universality of the existence of the complexity dual at late times in 4D. Notably, the smallest radius to which the extremal surface extends always approaches a constant value at late times. This guarantees the finite asymptotic value of the conserved momentum and thus a constant increasing rate of the volume-complexity at late times. We observed that starting from the boundary time $\tau = 0$, the conserved momentum grows monotonically and the minimal radius of the extremal surface decreases monotonically to their corresponding finite asymptotic values at the local maximum of the effective potential. In cases where multiple local maxima co-exist, depending on the shape of the effective potential, phase transitions of the extremal surface can emerge if the local maximum closer to the singularity has a larger peak value than the outermost one. Otherwise, the extremal slice follows a similar pattern as in the single-peak potential. Furthermore, we demonstrated that dipping slices, on which P_ν decreases with time, do not yield the largest generalized volume and can be disregarded in the computation. We argued that this feature extends beyond the Gauss-Bonnet gravity and is solely determined by the shape of the effective potential of a specific model.

The Gauss-Bonnet gravity in 4D and higher dimensions are dramatically different; the 4D gravity has time-like singularities and higher-D models all exhibit space-like singularities. In the 5D case, we showed that the universality of extremal slices at late times observed in 4D is not present, and only models with certain finite range of coupling parameters can serve as viable duals to the complexity. However, for coupling parameters outside the range, one can nevertheless evaluate the generalized volume according to the proposed formula. However, we found that the extremal surface only exists for a finite boundary time in this scenario and cannot replicate the constant growing feature of the complexity at late times.

In summary, we investigated the CAny proposal in the Gauss-Bonnet gravity and extended the discussion to include the phase transitions of the extremal slices as well as the deformations of the extremal slices in various scenarios in the Gauss-Bonnet-AdS gravity. This study may stimulate further quest for the understanding of the quantum nature of gravity and shed light to the interiors of the black holes.

Acknowledgments

X.W would like to thank Yu-Sen An for helpful discussions and acknowledge the support of the start-up grant from the Wenzhou Institute of University of Chinese Academy of Sciences.

References

- [1] A. Almheiri, T. Hartman, J. Maldacena, E. Shaghoulian, and A. Tajdini, *The entropy of Hawking radiation*, *Rev. Mod. Phys.* **93** (2021), no. 3 035002, [[arXiv:2006.06872](#)].
- [2] D. N. Page, *Average entropy of a subsystem*, *Phys. Rev. Lett.* **71** (1993) 1291–1294, [[gr-qc/9305007](#)].
- [3] D. N. Page, *Information in black hole radiation*, *Phys. Rev. Lett.* **71** (1993) 3743–3746, [[hep-th/9306083](#)].
- [4] T. Hartman and J. Maldacena, *Time Evolution of Entanglement Entropy from Black Hole Interiors*, *JHEP* **05** (2013) 014, [[arXiv:1303.1080](#)].
- [5] L. Susskind, *Computational Complexity and Black Hole Horizons*, *Fortsch. Phys.* **64** (2016) 24–43, [[arXiv:1403.5695](#)]. [Addendum: *Fortsch.Phys.* 64, 44–48 (2016)].
- [6] D. Stanford and L. Susskind, *Complexity and Shock Wave Geometries*, *Phys. Rev. D* **90** (2014), no. 12 126007, [[arXiv:1406.2678](#)].
- [7] J. Couch, W. Fischler, and P. H. Nguyen, *Noether charge, black hole volume, and complexity*, *JHEP* **03** (2017) 119, [[arXiv:1610.02038](#)].
- [8] A. Belin, R. C. Myers, S.-M. Ruan, G. Sárosi, and A. J. Speranza, *Does Complexity Equal Anything?*, *Phys. Rev. Lett.* **128** (2022), no. 8 081602, [[arXiv:2111.02429](#)].
- [9] A. Belin, R. C. Myers, S.-M. Ruan, G. Sárosi, and A. J. Speranza, *Complexity equals anything II*, *JHEP* **01** (2023) 154, [[arXiv:2210.09647](#)].
- [10] M.-T. Wang, H.-Y. Jiang, and Y.-X. Liu, *Generalized Volume-Complexity for RN-AdS Black Hole*, [[arXiv:2304.05751](#)].
- [11] R.-Q. Yang, *Strong energy condition and complexity growth bound in holography*, *Phys. Rev. D* **95** (2017), no. 8 086017, [[arXiv:1610.05090](#)].
- [12] Y.-S. An, R.-G. Cai, and Y. Peng, *Time Dependence of Holographic Complexity in Gauss-Bonnet Gravity*, *Phys. Rev. D* **98** (2018), no. 10 106013, [[arXiv:1805.07775](#)].
- [13] A. Ghodsi, S. Qolibikloo, and S. Karimi, *Holographic complexity in general quadratic curvature theory of gravity*, *Eur. Phys. J. C* **80** (2020), no. 10 920, [[arXiv:2005.08989](#)].
- [14] T. Mandal, A. Mitra, and G. S. Punia, *Action complexity of charged black holes with higher derivative interactions*, *Phys. Rev. D* **106** (2022), no. 12 126017, [[arXiv:2205.11201](#)].
- [15] H. Babaei-Aghbolagh, D. M. Yekta, K. Velni Babaei, and H. Mohammadzadeh, *Complexity growth in Gubser–Rocha models with momentum relaxation*, *Eur. Phys. J. C* **82** (2022), no. 4 383, [[arXiv:2112.10725](#)].
- [16] R.-G. Cai, S. He, S.-J. Wang, and Y.-X. Zhang, *Revisit on holographic complexity in two-dimensional gravity*, *JHEP* **08** (2020) 102, [[arXiv:2001.11626](#)].

- [17] S. A. Hosseini Mansoori and M. M. Qaemmaqami, *Complexity growth, butterfly velocity and black hole thermodynamics*, *Annals Phys.* **419** (2020) 168244, [[arXiv:1711.09749](#)].
- [18] R. Auzzi, G. Nardelli, G. P. Ungureanu, and N. Zenoni, *Volume complexity of dS bubbles*, *Phys. Rev. D* **108** (2023), no. 2 026006, [[arXiv:2302.03584](#)].
- [19] R. Emparan, A. M. Frassino, M. Sasieta, and M. Tomašević, *Holographic complexity of quantum black holes*, *JHEP* **02** (2022) 204, [[arXiv:2112.04860](#)].
- [20] H. Zolfi, *Complexity and Multi-boundary Wormholes in $2 + 1$ dimensions*, *JHEP* **04** (2023) 076, [[arXiv:2302.07522](#)].
- [21] Z.-Y. Fan and M. Guo, *Holographic complexity and thermodynamics of AdS black holes*, *Phys. Rev. D* **100** (2019) 026016, [[arXiv:1903.04127](#)].
- [22] J. Haferkamp, P. Faist, N. B. Kothakonda, J. Eisert, and N. Yunger Halpern, *Linear growth of quantum circuit complexity*, *Nature Physics* **18** (2022), no. 5 528–532.
- [23] J. Maldacena and L. Susskind, *Cool horizons for entangled black holes*, *Fortsch. Phys.* **61** (2013) 781–811, [[arXiv:1306.0533](#)].
- [24] A. R. Brown, D. A. Roberts, L. Susskind, B. Swingle, and Y. Zhao, *Complexity, action, and black holes*, *Phys. Rev. D* **93** (2016), no. 8 086006, [[arXiv:1512.04993](#)].
- [25] A. R. Brown, D. A. Roberts, L. Susskind, B. Swingle, and Y. Zhao, *Holographic Complexity Equals Bulk Action?*, *Phys. Rev. Lett.* **116** (2016), no. 19 191301, [[arXiv:1509.07876](#)].
- [26] D. Carmi, R. C. Myers, and P. Rath, *Comments on Holographic Complexity*, *JHEP* **03** (2017) 118, [[arXiv:1612.00433](#)].
- [27] A. Mounim and W. Mück, *Reparametrization dependence and holographic complexity of black holes*, *Phys. Rev. D* **105** (2022), no. 2 026024, [[arXiv:2106.01897](#)].
- [28] S. N. Sajadi and M. R. Setare, *Action-complexity in GMMG and EGMG*, *Gen. Rel. Grav.* **54** (2022), no. 12 157.
- [29] T. Anegawa, N. Iizuka, S. K. Sake, and N. Zenoni, *Is action complexity better for de Sitter space in Jackiw-Teitelboim gravity?*, *JHEP* **06** (2023) 213, [[arXiv:2303.05025](#)].
- [30] K. Meng, *Holographic complexity of Born–Infeld black holes*, *Eur. Phys. J. C* **79** (2019), no. 12 984, [[arXiv:1810.02208](#)].
- [31] F. Omid, *Regularizations of Action-Complexity for a Pure BTZ Black Hole Microstate*, *JHEP* **07** (2020) 020, [[arXiv:2004.11628](#)].
- [32] A. Akhavan and F. Omid, *On the Role of Counterterms in Holographic Complexity*, *JHEP* **11** (2019) 054, [[arXiv:1906.09561](#)].
- [33] M. Bravo-Gaete and F. F. Santos, *Complexity of four-dimensional hairy anti-de-Sitter black holes with a rotating string and shear viscosity in generalized scalar–tensor theories*, *Eur. Phys. J. C* **82** (2022), no. 2 101, [[arXiv:2010.10942](#)].
- [34] M. Alishahiha, K. Babaei Velni, and M. R. Mohammadi Mozaffar, *Black hole subregion action and complexity*, *Phys. Rev. D* **99** (2019), no. 12 126016, [[arXiv:1809.06031](#)].
- [35] D. M. Yekta, H. Babaei-Aghbolagh, K. Babaei Velni, and H. Mohammadzadeh, *Holographic complexity for black branes with momentum relaxation*, *Phys. Rev. D* **104** (2021), no. 8 086025, [[arXiv:2009.01340](#)].

- [36] E. Jørstad, R. C. Myers, and S.-M. Ruan, *Complexity=Anything: Singularity Probes*, [arXiv:2304.05453](#).
- [37] S. E. Aguilar-Gutierrez, M. P. Heller, and S. Van der Schueren, *Complexity = Anything Can Grow Forever in de Sitter*, [arXiv:2305.11280](#).
- [38] H.-Y. Jiang, M.-T. Wang, and Y.-X. Liu, *Holographic Complexity with Different Gravitational Observables*, [arXiv:2307.09223](#).
- [39] F. Omid, *Generalized volume-complexity for two-sided hyperscaling violating black branes*, *JHEP* **01** (2023) 105, [[arXiv:2207.05287](#)].
- [40] P. G. Fernandes, P. Carrilho, T. Clifton, and D. J. Mulryne, *The 4d einstein–gauss–bonnet theory of gravity: a review*, *Classical and Quantum Gravity* **39** (2022), no. 6 063001.
- [41] D. Glavan and C. Lin, *Einstein-gauss-bonnet gravity in four-dimensional spacetime*, *Physical review letters* **124** (2020), no. 8 081301.
- [42] P. G. S. Fernandes, P. Carrilho, T. Clifton, and D. J. Mulryne, *Derivation of Regularized Field Equations for the Einstein-Gauss-Bonnet Theory in Four Dimensions*, *Phys. Rev. D* **102** (2020), no. 2 024025, [[arXiv:2004.08362](#)].
- [43] N. Dadhich, *On causal structure of 4D-Einstein–Gauss–Bonnet black hole*, *Eur. Phys. J. C* **80** (2020), no. 9 832, [[arXiv:2005.05757](#)].
- [44] S.-W. Wei, Y.-X. Liu, and R. B. Mann, *Black Hole Solutions as Topological Thermodynamic Defects*, *Phys. Rev. Lett.* **129** (2022), no. 19 191101, [[arXiv:2208.01932](#)].
- [45] C. Liu and J. Wang, *Topological natures of the Gauss-Bonnet black hole in AdS space*, *Phys. Rev. D* **107** (2023), no. 6 064023, [[arXiv:2211.05524](#)].
- [46] R. Li, C. Liu, K. Zhang, and J. Wang, *Topology of the landscape and dominant kinetic path for the thermodynamic phase transition of the charged Gauss-Bonnet AdS black holes*, [arXiv:2302.06201](#).
- [47] R. Li and J. Wang, *Generalized free energy landscapes of the charged Gauss-Bonnet AdS black holes in diverse dimensions*, [arXiv:2304.03425](#).
- [48] R. Li and J. Wang, *Energy and entropy compensation, phase transition and kinetics of four dimensional charged Gauss-Bonnet Anti-de Sitter black holes on the underlying free energy landscape*, *Nucl. Phys. B* **976** (2022) 115714, [[arXiv:2012.05424](#)].
- [49] D. G. Boulware and S. Deser, *String Generated Gravity Models*, *Phys. Rev. Lett.* **55** (1985) 2656.
- [50] A. Buchel and R. C. Myers, *Causality of holographic hydrodynamics*, *Journal of High Energy Physics* **2009** (2009), no. 08 016.